JACS
JOURNAL OF THE AMERICAN CHEMICAL SOCIETY

Article

pubs.acs.org/JACS

Function of the Diiron Cluster of *Escherichia coli* Class Ia Ribonucleotide Reductase in Proton-Coupled Electron Transfer

Bigna Wörsdörfer,[†] Denise A. Conner,[†] Kenichi Yokoyama,[§] Jovan Livada,[†] Mohammad Seyedsayamdost,[§] Wei Jiang,[†] Alexey Silakov,*[,†] JoAnne Stubbe,*[,§,∥] J. Martin Bollinger, Jr.,*[,†,‡] and Carsten Krebs*[,†,‡]

[†]Department of Chemistry and [‡]Department of Biochemistry and Molecular Biology, The Pennsylvania State University, University Park, Pennsylvania 16802, United States

[§]Department of Chemistry and [∥]Department of Biology, Massachusetts Institute of Technology, Cambridge, Massachusetts 02139, United States

Supporting Information

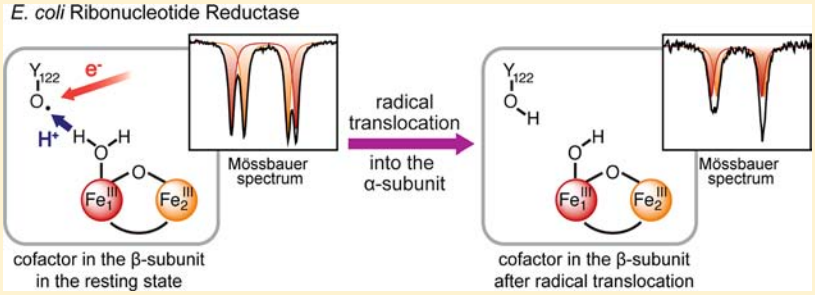

ABSTRACT: The class Ia ribonucleotide reductase (RNR) from *Escherichia coli* employs a free-radical mechanism, which involves bidirectional translocation of a radical equivalent or "hole" over a distance of ∼35 Å from the stable diferric/tyrosyl-radical ($Y_{122}^{\bullet}$) cofactor in the β subunit to cysteine 439 (C_{439}) in the active site of the α subunit. This long-range, intersubunit electron transfer occurs by a multistep "hopping" mechanism via formation of transient amino acid radicals along a specific pathway and is thought to be conformationally gated and coupled to local proton transfers. Whereas constituent amino acids of the hopping pathway have been identified, details of the proton-transfer steps and conformational gating within the β sununit have remained obscure; specific proton couples have been proposed, but no direct evidence has been provided. In the key first step, the reduction of $Y_{122}^{\bullet}$ by the first residue in the hopping pathway, a water ligand to Fe_1 of the diferric cluster was suggested to donate a proton to yield the neutral Y_{122}. Here we show that forward radical translocation is associated with perturbation of the Mössbauer spectrum of the diferric cluster, especially the quadrupole doublet associated with Fe_1. Density functional theory (DFT) calculations verify the consistency of the experimentally observed perturbation with that expected for deprotonation of the Fe_1-coordinated water ligand. The results thus provide the first evidence that the diiron cluster of this prototypical class Ia RNR functions not only in its well-known role as generator of the enzyme's essential $Y_{122}^{\bullet}$, but also directly in catalysis.

INTRODUCTION

Ribonucleotide reductases (RNRs) catalyze the reduction of ribonucleotides to deoxyribonucleotides in all organisms, thereby providing and controlling the only de novo pathway to the four precursors required for DNA replication and repair.[1,2] RNRs use a free-radical mechanism, in which a transient cysteine thiyl radical ($C^{\bullet}$) in the active site of the enzyme initiates substrate reduction by abstraction of a hydrogen atom ($H^{\bullet}$) from C3′.[1,3−9] In class Ia RNRs, such as the RNR from aerobically growing *Escherichia coli* (*E. coli*), a stable tyrosyl radical ($Y_{122}^{\bullet}$ in the *E. coli* ortholog) in close proximity to a μ-oxo-$(Fe^{III})_2$ cluster in the β subunit[10−14] reversibly generates the transient $C^{\bullet}$ in the active site of the enzyme's α subunit in the functional $\alpha_2\beta_2$ complex.[5−7,15,16] A model of the complex, constructed by computer docking of the structures of the individual subunits[7] and subsequently validated by electron−electron double resonance spectroscopic experiments,[17−19] suggests a distance of ∼35 Å between $Y_{122}^{\bullet}$ in β and the $H^{\bullet}$-abstracting C_{439} in α. Electron transfer (ET) between C_{439} and Y_{122} by a single tunneling step over that distance would be far too slow to account for the enzyme's turnover rate (2−10 s^{-1}).[15,20] Instead, this long-range intersubunit ET is mediated by a chain of strictly conserved aromatic amino acids, which form transient radicals in a "hopping" mechanism (Scheme 1A).[7,15,21−28] Direct detection of these pathway radicals in the wild-type enzyme has been hampered by a preceding rate-limiting conformational change within the $\alpha_2\beta_2$ complex.[20] This slow conformational change, which occurs upon binding of substrate and allosteric effector

Received: February 10, 2013
Published: May 16, 2013

 © 2013 American Chemical Society

Scheme 1. (A) Proposed Radical Translocation Pathway and (B,C) Schematic Representation of the Two Approaches Used To Trap the Forward Radical Translocation Product in *E. coli* RNR[a]

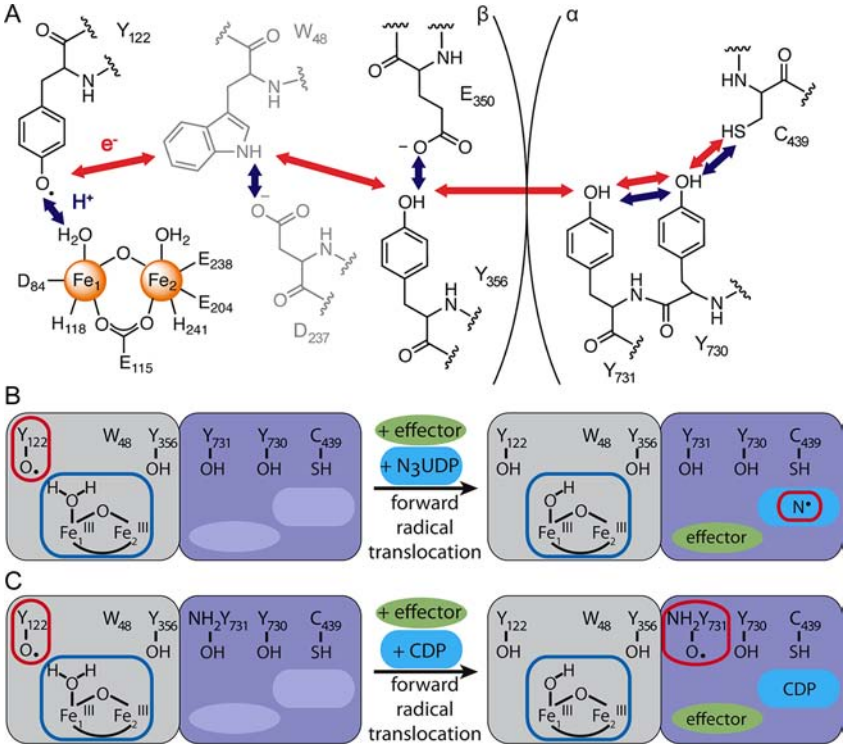

[a]In (A) W_{48} and D_{237} are shown in gray because there is currently no direct evidence for involvement of W_{48} in radical translocation. Trapping of the forward radical translocation product induced by N_3UDP in the wild-type $\alpha_2\beta_2$ complex is shown in (B), and by CDP in a complex with an α variant containing the radical-stabilizing unnatural amino acid 3-aminotyrosine (NH_2–Y) at residue α-Y_{731} is shown in (C). EPR- and Mössbauer-observable species are illustrated in (B) and (C) by red and blue outlines, respectively.

to α and allows for translocation of the radical from its resting location on β-Y_{122} to where it functions in catalysis on α-C_{439}, masks the subsequent, fast chemical events.[20] Substitution of pathway tyrosines by unnatural amino acids with altered redox properties led to the first detection of pathway radicals and provided the most direct evidence that these residues are redox-active "stepping stones" in the long-range ET (Scheme 1A).[21−26] The individual ET hopping steps in the overall 35 Å hole-translocation process are thought to be coupled to multiple short-range proton transfer steps (i.e., proton-coupled ET or PCET), which effectively tune the thermodynamics of the component steps for efficiency and reversibility of the overall process.[15,29] The coupling of ET to proton transfer (PT) steps could therefore permit radical translocation to be controlled by the PT steps, which could, due to their more stringent distance and orientation requirements, be controlled by the conformation of the protein: engagement of a proton-transfer pathway upon substrate binding could be the basis for the conformational gating in RNR.

Whereas the radical-hopping nature of the process and the identities of the mediating residues have (with the exception of tryptophan 48 in β, which may or may not be a mediator) been established, much less is known about the details of the proton transfers. It has been proposed that PT proceeds orthogonally to ET in the β subunit and collinearly in α.[15,29] A recent electron−nuclear double resonance (ENDOR) spectroscopic study provided evidence for hydrogen bonds among the three ET pathway residues of α in the active $\alpha_2\beta_2$ complex, consistent with collinear PCET.[30] Within the β subunit, specific proton coupling partners have been proposed (Scheme 1A), but little experimental evidence has been provided.[27,31] Specifically, in the first step of forward (β-$Y_{122}^{\bullet}$ → α-C_{439}) radical translocation, the neutral $Y_{122}^{\bullet}$ is reduced to the neutral Y_{122} by β-Y_{356} (or perhaps β-W_{48}) in the pathway, and it has been suggested that the proton required to maintain neutrality of the Y_{122} side chain is delivered orthogonally to ET by the water ligand on the iron ion in site 1 (Fe_1).[15,32] In this study, we have trapped the cofactor in β in its product state of the forward radical translocation process by using either the radical-trapping substrate analogue 2′-azido-2′-deoxyuridine 5′-diphosphate (N_3UDP) with the wild-type enzyme or a natural substrate (CDP) with a variant of the α-subunit containing the radical-stabilizing unnatural amino acid 3-aminotyrosine (NH_2–Y) at the subunit-interfacial pathway residue α-Y_{731} (Scheme 1B and C). We show that the Mössbauer spectrum of the $(Fe^{III})_2$ cluster, especially the quadrupole splitting parameter (ΔE_Q) associated with Fe_1, changes while the oxidation state of the cluster remains unchanged and that this spectral perturbation is specific to the form of the enzyme that has engaged in forward radical translocation. The nature of the observed perturbation—an approximately 0.5 mm/s diminution in $|\Delta E_Q|$ of Fe_1 with much smaller changes to $|\Delta E_Q|$ of Fe_2 and the isomer shifts (δ) of both sites—agrees remarkably well with the effect predicted by simple DFT calculations for removal of a proton from the Fe_1–OH_2 ligand. The results provide the first direct evidence that the diiron cluster of the prototypical class Ia RNR from *E. coli* not only serves its well-known role as generator of the $Y_{122}^{\bullet}$ [11,15,33] but also actively participates in the enzyme's catalytic cycle.

dx.doi.org/10.1021/ja401342s | J. Am. Chem. Soc. 2013, 135, 8585−8593

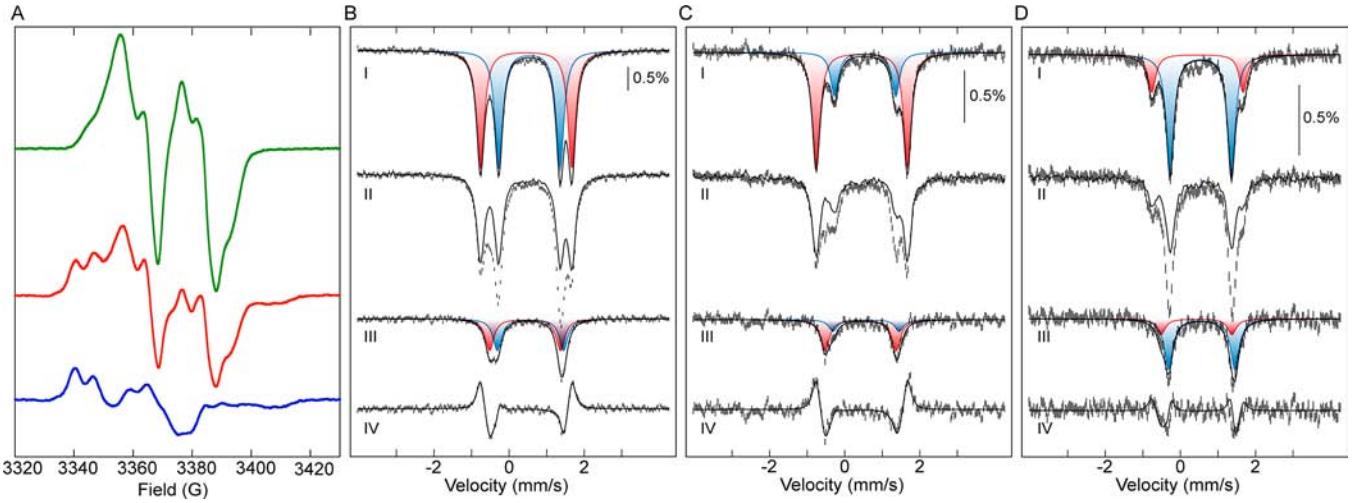

Figure 1. EPR and Mössbauer spectra of *E. coli* RNR before and after N_3UDP-induced trapping of the product of forward radical translocation. (A) EPR spectra of uniformly ^{57}Fe-labeled $\alpha_2\beta_2$ with TTP and in the absence (green) or presence (red) of N_3UDP. Subtraction of the features of the unreacted $Y_{122}^{\bullet}$ (green) from the spectrum of the N_3UDP-treated sample (red) yields the spectrum of the $N^{\bullet}$ (blue). 4.2-K/53-mT Mössbauer spectra of uniformly ^{57}Fe-labeled (B), site 1 ^{57}Fe-enriched (C), and site 2 ^{57}Fe-enriched (D) $\alpha_2\beta_2$ with TTP and in the absence (I) or presence (II) of N_3UDP. The solid lines in I are simulations of the two quadrupole doublets (red and blue) of the resting $(Fe^{III})_2$ cluster with parameters quoted in the text and the sum of the two doublets (black). The solid line in II is the spectrum from I scaled appropriately to remove the contribution of the unreacted cofactor. Subtraction of this contribution from II reveals the spectrum of the product of the forward radical translocation (III), which can be simulated with two quadrupole doublets (red and blue; parameters quoted in the text). The sum of the two quadrupole doublet simulations is shown as a black line. The spectrum in IV is the total difference of I−II, and the solid line is a simulation of the difference spectrum as a sum of the four quadrupole-doublet components.

RESULTS AND DISCUSSION

To initiate forward radical translocation and trap the enzyme in the product state of this step, the α and β subunits were incubated in the presence of the positive allosteric effector, thymidine triphosphate (TTP), with the substrate analogue N_3UDP, which brings about the irreversible reduction of $Y_{122}^{\bullet}$ in β along with the formation of a metastable, nucleotide-based, nitrogen-centered radical ($N^{\bullet}$) in the active site of α (Scheme 1B).[34−36] Conversion of β-$Y_{122}^{\bullet}$ to the $N^{\bullet}$ was confirmed by comparison of the X-band EPR spectrum at 14 K of the reaction sample (Figure 1A, red) to that of a control sample from which N_3UDP was omitted (Figure 1A, green). Subtraction of the features of the unreacted β-$Y_{122}^{\bullet}$ from the spectrum of the N_3UDP-treated sample yields the spectrum of the $N^{\bullet}$ (Figure 1A).[36,37] Its intensity accounts for ∼36% of the $Y_{122}^{\bullet}$ originally present in the control (−N_3UDP) sample. Conversions of ≤50% have generally been observed in such experiments with *E. coli* RNR and have been attributed to the facile reaction of only one $\alpha\beta$ pair in the $\alpha_2\beta_2$ heterotetramer ("half-of-sites reactivity"), a property thought to be intrinsic to the enzyme.[17,23−26]

The changes to the $(Fe^{III})_2$ cluster in β upon this N_3UDP-induced forward radical translocation were monitored by Mössbauer spectroscopy on two samples identical to the aforementioned EPR samples. The 4.2-K/53-mT Mössbauer spectrum of the control sample in the absence of N_3UDP [i.e., of the resting $(Fe^{III})_2$ cluster][38−40] consists of two resolved quadrupole doublets with parameters [isomer shift, δ_1, of 0.46 mm/s and quadrupole splitting parameter, ΔE_{Q1}, of 2.43 mm/s (Figure 1B, I, red), and δ_2 = 0.54 mm/s, ΔE_{Q2} = 1.63 mm/s (Figure 1B, I, blue)] nearly identical to those reported for active β alone and previously assigned to Fe_1 and Fe_2, respectively.[11,39,41,42] Incubation with N_3UDP changes the Mössbauer spectrum significantly, and the spectrum exhibits new features (Figure 1B, II, and clearly apparent in the difference spectrum, IV). Removal of the contribution of the unreacted $(Fe^{III})_2$ cluster by subtraction of the appropriately scaled spectrum of the control (−N_3UDP) sample (solid line) resolves the new spectrum of the radical translocation product (Figure 1B, III). The new features account for ∼41% conversion of the active cofactor, which agrees well with the conversion of $Y_{122}^{\bullet}$ to $N^{\bullet}$ determined by EPR (see also Table S2). The derived spectrum of the radical translocation product can be analyzed as two symmetrical quadrupole doublets with equal intensity and equal line width, and parameters δ_1 = 0.43 mm/s, ΔE_{Q1} = 1.89 mm/s, and δ_2 = 0.57 mm/s, ΔE_{Q2} = 1.76 mm/s (Figure 1B, III, red and blue, respectively; Table S1).[43] The modest changes to the isomer shifts of both sites and the fact that the spectrum still comprises quadrupole doublet features indicative of an integer-electron-spin ground state imply that no change in oxidation state of the $(Fe^{III})_2$ cluster is effected by the N_3UDP treatment,[44] as expected from previous studies employing this compound.[34−36] In addition, the large magnitudes of the ΔE_Q-values further suggest that the oxo bridge remains intact.[45]

The spectra of control samples containing β, effector, either CDP or N_3UDP, and an α variant having the hopping pathway disabled by substitution of the subunit-interfacial Y_{731} in α with F lack these new features and are essentially identical to the spectrum of the sample with wild-type α and β before reaction with N_3UDP (Figure S2). The spectrum of an additional control sample, in which the $Y_{122}^{\bullet}$ in β was reduced in the absence of α with hydroxyurea (HU) to yield the inactive $(Fe^{III})_2/Y_{122}$ met form (Figure S2),[46] is also very similar to that of the active form. These results imply that the observed perturbation to the spectrum of the $(Fe^{III})_2$ cluster in the wild-type enzyme caused by N_3UDP is related to radical translocation and not to either the absence of $Y_{122}^{\bullet}$ per se or nucleotide binding events.

dx.doi.org/10.1021/ja401342s | J. Am. Chem. Soc. 2013, 135, 8585−8593

The two quadrupole doublets that make up the spectrum of the radical translocation product were unambiguously assigned to Fe_1 and Fe_2 by site-selective labeling of β with ^{57}Fe and ^{56}Fe. The two sites in *E. coli* β have different affinities for Fe^{II}, and this property can be exploited to obtain β with the Mössbauer-active ^{57}Fe enriched in one or the other site.[41] The spectrum of a sample of the complex prepared with β subunit having site 1 enriched with ^{57}Fe can be simulated with the same parameters used for spectra of the uniformly ^{57}Fe-labeled samples above, and the relative intensities of the two quadrupole doublets indicate that ~73% of the ^{57}Fe resides in site 1 and ~27% in site 2 (Figure 1C, I, red and blue). Treatment of this sample with N_3UDP yielded a β-$Y_{122}^{\bullet}$ to $N^{\bullet}$ conversion of ~38%, as determined by EPR spectroscopy (Figure S3, Table S2), similar to that achieved with uniformly ^{57}Fe-labeled complex. The Mössbauer spectrum of the radical translocation product, obtained after subtraction of the unreacted component (Figure 1C, II and III), constitutes 38% of the active cofactor, in agreement with the EPR quantification. It can be simulated with the same parameters used for the spectrum of the product in the uniformly labeled complex (Figure 1C, III, red and blue). Owing to the site-selective labeling, the two quadrupole doublets have different intensities and can therefore be unambiguously assigned to Fe_1 (red) and Fe_2 (blue). Samples with ^{57}Fe enriched in site 2 confirm this assignment (Figure 1D). These samples contain ~24% of the ^{57}Fe in site 1 and ~76% in site 2 (Figure 1D, I, red and blue). Reaction with N_3UDP resulted in conversion of ~47% of initial β-$Y_{122}^{\bullet}$ to $N^{\bullet}$, as quantified by EPR (Figure S3, Table S2), and produced the Mössbauer spectrum shown in Figure 1D, II. The Mössbauer spectrum of the radical translocation product, obtained after removal of the unreacted component (Figure 1D, III) and accounting for 52% conversion of the active cofactor, can again be simulated with the same parameters used for the spectrum of the product with the uniformly and site-1-enriched complexes (Figure 1D, III, red and blue). Assignment of the two quadrupole doublets to Fe_1 (red) and Fe_2 (blue) shows that the spectrum of Fe_1, the site with the water proposed to be the proton donor, changes much more ($|\Delta E_Q|$ decreases by 0.5 mm/s) than that of Fe_2 upon N_3UDP-induced trapping of the radical translocation product.

In addition to the use of the radical-trapping substrate analogue, N_3UDP, the product of forward radical translocation can also be trapped by using an α variant that contains an unnatural amino acid incorporated into the hopping pathway (Scheme 1C). The radical produced from 3-aminotyrosine ($NH_2Y^{\bullet}$) has a reduction potential estimated to be ~190 mV less than that of $Y^{\bullet}$, causing the radical to reside on this unnatural residue during catalysis by *E. coli* RNR variants.[23,47] The variant α protein having NH_2Y in place of Y_{731} is capable of nucleotide reduction, and upon its incubation with the β subunit, the effector ATP and the CDP substrate, a $NH_2Y^{\bullet}$ accumulates to ~50% of the total spin in the sample.[23] The dependence on the presence of nucleotides and β, and the ability of this enzyme to catalyze deoxynucleotide production, show that the $NH_2Y^{\bullet}$ forms by gated radical translocation in the functional holoenzyme complex. Translocation of the radical from β-$Y_{122}^{\bullet}$ to α-NH_2Y_{731} is expected to be accompanied by the same change to the $(Fe^{III})_2$ cluster observed above in the wild-type complex upon reaction with N_3UDP. Indeed, the experimental Mössbauer spectrum after reaction of β with α-$Y_{731}NH_2Y$, ATP, and CDP and the product spectrum (45% conversion) obtained after removal of the unreacted component (Figure 2) are almost identical to the spectra of the radical translocation product trapped by N_3UDP (Figure 1B). The observation of the same perturbed quadrupole-doublet spectrum in samples in which the $Y_{122}^{\bullet}$-reduced β was trapped by either N_3UDP or the α-$Y_{731}NH_2Y$ variant, but not in samples prepared either with a pathway-disabled α or by reduction of $Y_{122}^{\bullet}$ by HU in the absence of α, strongly suggests that the change to the $(Fe^{III})_2$ cluster is associated specifically with functional translocation of the radical from $Y_{122}^{\bullet}$ into the hopping pathway.

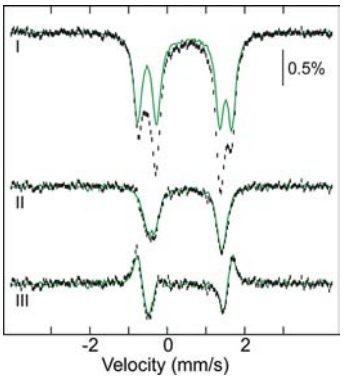

Figure 2. 4.2-K/53-mT Mössbauer spectrum of the product of forward radical translocation trapped in the $(Y_{731}NH_2Y\text{-}\alpha)_2\beta_2$ complex. (I) Sample prepared with β, $Y_{731}NH_2Y$-α, ATP, and CDP. The green line is the scaled control spectrum of β that had been incubated with pathway-blocked $Y_{731}F$-α, ATP, and CDP, and subtraction of this spectral contribution reveals the spectrum of the product of forward radical translocation (II). The green line overlaid in II is the spectrum of the radical translocation product induced with N_3UDP from Figure 1B, III, and is shown to illustrate the near identity of the perturbed spectra resolved by the two different trapping approaches. The spectrum in III is the total difference of the spectrum of $(Y_{731}F\text{-}\alpha)_2\beta_2$ in the presence of ATP and CDP subtracted from I, and the green line is the total difference spectrum from the $\alpha_2\beta_2 \pm N_3UDP$ experiment in Figure 1B, IV.

To evaluate whether the change to the Mössbauer spectrum of the diferric cluster observed upon radical translocation is consistent with the proposed deprotonation of the $Fe_1{-}OH_2$ (Scheme 1B and C), we performed a series of DFT calculations. Remarkably, the calculations, performed by the broken-symmetry DFT methodology,[48] predict the same qualitative change to the Mössbauer parameters upon removal of a proton from the $Fe_1{-}OH_2$ [0.47–0.74 mm/s decrease in $|\Delta E_Q|$ for Fe_1, a much smaller (≤0.25 mm/s) increase or decrease in $|\Delta E_Q|$ of Fe_2, and almost no change (0.04 mm/s) to the isomer shift of either site; Figure 3 and Table S3] as is observed experimentally upon radical translocation. The calculations were performed by starting from the published high-resolution structure of the *E. coli* β protein,[49] which is purportedly of the met form. All first-sphere (ligand) residues and nonprotein oxygen ligands [an HO(H) ligand to each iron and the oxo bridge] were included in the models (Figure S4). Two sets of models were considered. One set includes both the diferric cluster and the radical tyrosine (Y_{122}) in either the resting state of the cofactor ($Fe_1{-}OH_2/Y^{\bullet}$) or the postulated radical-translocation-product state ($Fe_1{-}OH/Y$). A second set includes the diferric cluster in either its resting ($Fe_1{-}OH_2$) or radical translocation ($Fe_1{-}OH$) state but omits the tyrosine (Figure S4). To limit the number of atoms while still preventing ligand motions that would be precluded by their attachment to the protein backbone from occurring during

dx.doi.org/10.1021/ja401342s | J. Am. Chem. Soc. 2013, 135, 8585–8593

geometry optimization, the approach used by Roos and Siegbahn was adopted.[50] With these geometric constraints, none of the calculated models diverged markedly from the experimental structure during optimization (Figure S4). In addition to calculations in the gas phase, the effect of the protein environment on the calculated Mössbauer parameters was evaluated using the COSMO solvation model[51,52] with various dielectric constants (ε) of 4, 10, and 40. Calculations using ε = 4 reproduce the experimental parameters remarkably well, to within ±0.18 mm/s for the models that include Y_{122} (Figure 3A). Moreover, all of the calculations, whether in the gas phase or with the COSMO solvent model and with Y_{122} included or omitted, reproduce the essential features of the experimental spectral perturbation, giving a relatively large decrease in $|\Delta E_Q|$ and much smaller change in δ for site 1 and small changes in $|\Delta E_Q|$ and δ for site 2 (Figure 3B and Table S3). The results imply that the observed effect arises directly from the change in the charge of the Fe_1 HO(H) ligand rather than some interaction of the cluster with the $Y_{122}/Y_{122}^{\bullet}$. Consistent with this conclusion and the experimental Mössbauer spectra, parameters calculated for a model having the reduced, neutral Y_{122} and the Fe_1−OH_2 ligand (corresponding to the met form of the protein) do not deviate significantly from those calculated for the active state (with $Y_{122}^{\bullet}$ and Fe_1−OH_2). These DFT calculations thus establish that the change to the Mössbauer spectrum associated with radical translocation is consistent with the proposed donation of a proton to Y_{122} by the Fe_1−OH_2 in the first PCET step.

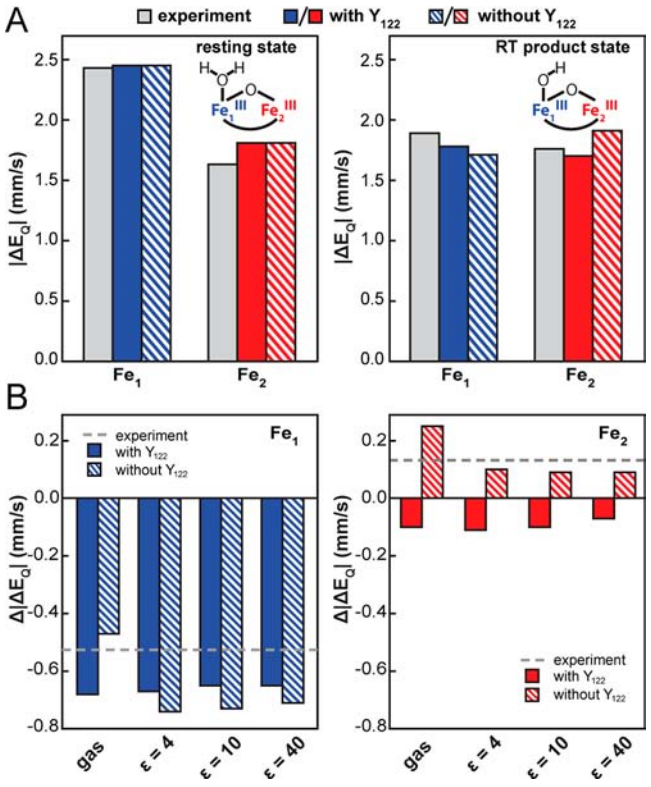

Figure 3. Comparison of the experimental quadrupole splitting (ΔE_Q) parameters for the resting and radical-transolcation-product states of the cofactor to the values calculated by DFT. (A) Absolute values of ΔE_Q from experiment (gray bars) and the DFT calculations using a dielectric constant of ε = 4 for models of either the full cofactor including Y_{122} (solid colored bars) or just the diferric cluster without Y_{122} (striped colored bars). The blue bars correspond to Fe_1 and the red bars to Fe_2. (B) The changes in the absolute values of ΔE_Q associated with the radical-translocation/deprotonation event either from the experiments (dashed gray lines) or from the calculations on the models including (solid bars) or omitting (striped bars) Y_{122}. The color coding is the same as in panel A.

We anticipated that the Fe_1−OH radical translocation product would be metastable and eventually undergo protonation (with the ultimate source being bulk solvent) to generate the Fe_1−OH_2 species of the stable met form (Fe_1−OH_2/Y). To test this notion, the radical translocation product trapped with N_3UDP was thawed and incubated on ice to permit decay of the $N^{\bullet}$ and enable subsequent adjustments of the protein complex and the $(Fe^{III})_2$ cluster. Periodically, the sample was refrozen for acquisition of its Mössbauer spectrum. Spectra acquired after total incubation times of 10−260 min demonstrate the return of the spectrum of the resting (presumably Fe_1−OH_2) form of the cluster (Figure 4). This result further confirms that the observed perturbation to the $(Fe^{III})_2$ cluster upon reaction with N_3UDP or $Y_{731}NH_2Y$-α and CDP is specific to the complex actively engaged in radical translocation and catalysis. The regeneration is relatively slow ($t_{1/2}$ of ∼60 min at ∼0 °C), consistent with the hypothesis that it reflects the slow diffusion of an extra proton from bulk solvent to the Fe_1−OH in the protein interior to convert it to Fe_1−OH_2 of the resting met form (perhaps subsequent to decay of the $N^{\bullet}$ and disengagement of β from α with a $t_{1/2}$ of 23 min at 25 °C[53]). That this proton transfer from bulk solvent would be slow is supported by studies in which the kinetics of electrochemical reduction of the β subunit in the presence of a facile ET mediator (methyl viologen) were monitored. These experiments revealed that the $(Fe^{III})_2$ center in the met form can be reduced relatively rapidly (within seconds), whereas

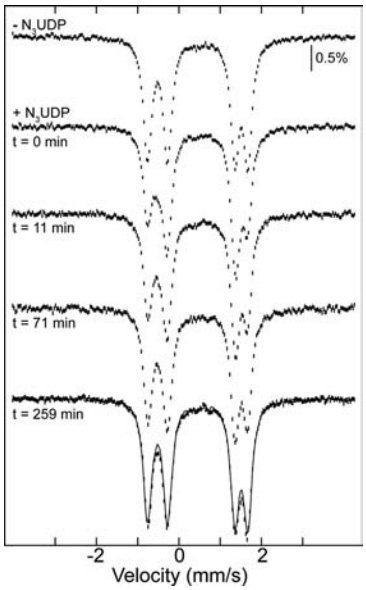

Figure 4. Conversion of the spectrum of the N_3UDP-trapped radical translocation product to that of the resting $(Fe^{III})_2$ cluster upon prolonged incubation on ice. 4.2-K/53-mT Mössbauer spectra of $\alpha_2\beta_2$ with TTP and in the absence or presence of N_3UDP. The +N_3UDP sample was thawed, incubated on ice, and periodically refrozen after total incubation times of 10−260 min for reacquisition of its Mössbauer spectrum. The spectrum at t = 260 min is almost identical to the spectrum of $\alpha_2\beta_2$ with TTP in the absence of N_3UDP (overlaid as a solid line).

dx.doi.org/10.1021/ja401342s | J. Am. Chem. Soc. 2013, 135, 8585−8593

reduction of the active $(Fe^{III})_2/Y_{122}^{\bullet}$ form of the protein proceeds with the initial fast reduction of $Y_{122}^{\bullet}$ followed by much slower reduction of the $(Fe^{III})_2$ cluster.[40] The observations suggest that the cluster in the met form and the one generated from the active $(Fe^{III})_2/Y_{122}^{\bullet}$ cofactor upon rapid $Y_{122}^{\bullet}$ reduction are somehow different. A reasonable explanation is that the cluster after fast $Y_{122}^{\bullet}$ reduction has the same number of protons as the radical translocation product, possessing the Fe_1−OH generated by transfer of a proton from the Fe−OH_2 to Y_{122} (Scheme 1B and C), whereas the stable met form produced by HU reduction of $Y_{122}^{\bullet}$ in the absence of α has the cluster in the Fe_1−OH_2 form. The absence of this proton in the initial $Y_{122}^{\bullet}$-reduced β and presence in the stable met form would make the charge of the buried cluster different by one unit, altering the electrostatics of the site and potentially causing the difference in reduction kinetics of the two forms.

CONCLUSION

The diiron cluster in class Ia *E. coli* RNR has long been known to generate the $Y_{122}^{\bullet}$ in the initial activation of the β subunit by reaction of its $(Fe^{II})_2$ form with O_2.[11,15,33] Our results now strongly suggest that the $(Fe^{III})_2$ cluster also actively functions in the catalytic cycle, specifically during translocation of the oxidizing equivalent or hole from its resting position on $Y_{122}^{\bullet}$ in β to the nucleotide reduction site in α. Reduction of $Y_{122}^{\bullet}$ upon forward radical translocation requires transfer of a proton to yield a neutral Y_{122}, and upon reverse radical translocation and reoxidation to $Y_{122}^{\bullet}$, the proton should be returned. The Mössbauer-detected change to the cluster seen upon use of either the substrate analog or the α variant is almost certainly associated specifically with propagation of the radical into the hopping pathway, because the perturbation (1) is observed when the radical on Y_{122} translocates in a functionally relevant reaction into α, but not when it is reduced in a nonfunctional context by HU, (2) relaxes upon decay of the $N^{\bullet}$ in α, and (3) is not observed in a complex having the hopping pathway blocked by the α-$Y_{731}F$ substitution. The nature of the spectral perturbation (significant decrease in $|\Delta E_Q|$ of site 1 and much smaller changes to the other three parameters) implies that the oxidation state of the cluster does not change and matches that predicted by DFT calculations for the removal of a proton from the Fe_1−OH_2 ligand. Our data are thus consistent with the previous suggestion that this water ligand serves as the proton-coupling partner to Y_{122} for radical translocation (Scheme 1).[15,32] The reduction of $Y_{122}^{\bullet}$ constitutes the first step of forward radical translocation and might, therefore, be a key step in the gating of the process by the protein. If one or more protein side chain is required to mediate this proton transfer (e.g., the nearby D_{84} carboxylate ligand), a conformational change in the $\alpha_2\beta_2$ complex occurring upon substrate binding could engage this proton-transfer pathway and thereby open the gate to reduction of $Y_{122}^{\bullet}$ by either W_{48} or Y_{356} in the initial step of the long-distance radical translocation.

METHODS

Materials, protein production and purification, reconstitution of RNR-β with ^{57}Fe and/or ^{56}Fe, and activity assays are described in the Supporting Information.

Reactions with N_3UDP. The reaction was carried out in a final volume of 0.6 mL and contained 0.3 mM α_2 (or 0.29 mM $Y_{731}F$-α_2), 0.3 mM β_2 (0.27 mM β_2 in the case of uniformly ^{57}Fe-labeled β and 0.29 mM β_2 in the case of $Y_{731}F$-α_2), 0.8 mM TTP, 1 mM N_3UDP, 15 mM $MgSO_4$, 1 mM EDTA, and 1 mM DTT in HEPES buffer. The reaction was initiated by the addition of N_3UDP and β_2 and allowed to proceed at RT (21 ± 2 °C) for a total reaction time of 2.5 min. Aliquots (0.3 mL) were transferred to Mössbauer and EPR sample cells and frozen in liquid N_2.

Reaction of $Y_{731}NH_2Y$-α_2 with Substrate. Prereduced $Y_{731}NH_2Y$-α_2 and ^{57}Fe-reconstituted β_2 in assay buffer were concentrated to 0.3 mL and mixed with an aliquot (0.05 mL) of ATP and CDP in assay buffer. The final reaction solution (0.35 mL) contained 0.25 mM $Y_{731}NH_2Y$-α_2, 0.25 mM β_2, 3 mM ATP, and 1 mM CDP and was incubated at RT (22 °C) for a total reaction time of 20 s and frozen in liquid N_2.

EPR Spectroscopy and Analysis. EPR spectra were recorded on a Bruker ESP300 spectrometer equipped with a ER 041 MR Microwave Bridge and a Bruker 4102ST TE_{102} X-band resonator. Spectrometer configuration and data acquisition were performed by an external PC via GPIB interface using EWWIN 6.1 software from Scientific Software Services. Spectra were acquired at a temperature of 14.0 ± 1 K, a microwave power of 8 μW, a microwave frequency of 9.45 GHz, a modulation amplitude of 3 G, a modulation frequency of 100 kHz, a receiver gain of 5×10^4, and a conversion time of 0.029 s. Four scans were averaged for the spectra acquired from 2000 to 4000 G. For spectra collected over the narrower field range from 3180 to 3580 G, a modulation amplitude of 1.0 G was used, and two scans were averaged.

The total electron spin concentration in each sample was determined by integrating its EPR absorption spectrum and comparing the integrated area to that of the spectrum of a standard containing 1.025 mM $CuSO_4$, 2 M $NaClO_4$, and 0.01 M HCl.[54] The first derivative spectra recorded from 2000 to 4000 gauss G were integrated, and the baselines were corrected by using a linear function. The second integral was formed, and integrated areas were corrected for differences in g-values, as previously described.[55]

Samples treated with N_3UDP contain a mixture of $Y_{122}^{\bullet}$ and the nitrogen-centered radical ($N^{\bullet}$). Removal of the features of the $Y_{122}^{\bullet}$ by subtraction of the appropriately scaled spectrum of the control (−N_3UDP) sample yields the spectrum of $N^{\bullet}$. Quantification of the subspectra of $Y_{122}^{\bullet}$ (scaled control spectrum) and $N^{\bullet}$ in the samples was accomplished by integrating the two subspectra, applying a linear baseline correction, and forming the second integral to determine the area. These areas were used to calculate the percent area of the two subspectra, which were then multiplied by the measured total spin concentration of the samples to determine the concentration of each radical. The values are reported in Table S2. The concentrations of the $Y_{122}^{\bullet}$ and $N^{\bullet}$ in the N_3UDP treated samples can also be calculated using the scaling factor of the $Y_{122}^{\bullet}$ control spectrum that was subtracted. This scaling factor was multiplied by the spin concentration of the control sample to determine the concentration of $Y_{122}^{\bullet}$ in the sample. This was then subtracted from the concentration of the reacted sample to determine the remaining spin concentration, which was attributed to $N^{\bullet}$. The values obtained by this procedure agree well with the values using the double integral of the two subspectra reported in Table S2.

Mössbauer Spectroscopy and Analysis. Mössbauer spectra were recorded at a temperature of 4.2 K in an externally applied magnetic field of 53 mT oriented parallel to the γ-beam on a SVT-400 spectrometer from WEB Research (Edina, MN). Data analysis was performed using WMOSS (WEB Research, Edina, MN). Isomer shifts are quoted relative to the centroid of a spectrum of a metallic foil of α-Fe at room temperature.

Parameters of the Spectrum of the Active $\alpha_2\beta_2$ Complex before Reaction. The Mössbauer spectrum of the active $\alpha_2\beta_2$ complex consists of two symmetrical quadrupole doublets of equal intensity. The spectrum was fitted by two quadrupole doublets with the linewidths (Γ) of the doublets constrained to be the same. The resulting parameters are cited in the main text and in Table S1.

Analysis of the Spectrum of the $\alpha_2\beta_2$ Complex after Reaction with N_3UDP. Removal of the contribution of the unreacted $(Fe^{III})_2$ cluster (71% of total Fe of the uniformly ^{57}Fe-labeled sample) from the spectrum of the sample reacted with N_3UDP resolves the spectrum of the radical translocation product. The subtraction was guided by

dx.doi.org/10.1021/ja401342s | J. Am. Chem. Soc. 2013, 135, 8585−8593

visual inspection of the resolved left line at −0.76 mm/s and by the objective of making the resulting spectrum symmetric. The spectrum of the radical translocation product was then analyzed as two symmetrical quadrupole doublets of equal intensity and line width. Two sets of physically meaningful parameters (left−right solution and inner−outer solution, Table S1) fit the data equally well and cannot be distinguished owing to the 1:1 ratio of the two quadrupole doublets.

The dependence of the Mössbauer parameters obtained for the radical translocation product on the fraction of the spectrum of unreacted complex subtracted from the experimental spectrum was evaluated. We found that δ and ΔE_Q vary by only 0.001−0.02 mm/s, which is within the intrinsic uncertainty limit for the parameters (0.02 mm/s), when reference spectra for the radical translocation product corresponding to 29 ± 3% of total Fe (71 ± 3% of the experimental spectrum attributed to the unreacted cluster and removed in the subtraction) were analyzed.

Analysis of the Spectra with Site-Selective ^{57}Fe-Labeled β. To determine the occupancies of ^{57}Fe in sites 1 and 2 in the site-selectively labeled βs, Mössbauer spectra of the $^{57}Fe_1$- and $^{57}Fe_2$-enriched β (1.3 mM β_2) used in all the experiments were recorded. The spectra were simulated by fixing the parameters to those obtained from analysis of the spectrum of the uniformly ^{57}Fe-labeled β in the sample of the $\alpha_2\beta_2$ complex and allowing only the areas of the two doublets to vary. The relative areas for the two doublets correspond to the relative amounts of ^{57}Fe in sites 1 and 2, respectively. These occupancies were kept constant for all subsequent analyses of the spectra of reaction samples.

Subtractions of the unreacted component (scaled spectra of $\alpha_2\beta_2$ before reaction) from the spectra after reaction with N_3UDP to obtain the spectrum of the radical translocation products were carried out as described above for the uniformly ^{57}Fe-labeled samples. The product spectrum was simulated with the same parameters as used for the spectrum of the product in the uniformly labeled complex but using the areas for the two quadrupole doublets determined above. To evaluate the robustness of the percentage of intensity assigned to the unreacted complex, theoretical spectra for the two quadrupole doublets of the radical translocation product (using the quoted parameters) were subtracted in appropriate fractions from product spectra generated by subtraction of different amounts of the unreacted component.

The spectra of the site-selectively labeled samples allow unambiguous assignment of the two quadrupole doublets to Fe_1 (red) and Fe_2 (blue). In addition, they should, in principle, allow differentiation between the two possible sets of parameters (left−right solution and inner−outer solution, Table S1). However, the parameters of the two solutions are very similar, and we cannot make this assignment with confidence. While the two low-energy lines are at least partially resolved, both solutions (inner−outer and left−right) assign the −0.52 mm/s and −0.31 mm/s lines to the quadrupole doublets associated with Fe_1 and Fe_2, respectively. For the high-energy lines, the two lines are nearly at the same position (1.37 and 1.45 mm/s). The small difference in line position of only of 0.08 mm/s precludes a distinction between the two solutions, because variations in the line width influence the simulations to a greater extent than the choice of inner−outer versus left−right parameters.

DFT Calculations. All geometry optimizations were performed using the Gaussian 09[56] revision C.01 package. The initial geometry guess was based on the crystal structure of *E. coli* RNR β, which is purportedly the diferric met form (PDB 1MXR[49]). First shell residues around the irons and Y_{122} were cut at the α carbon. To mimic the strain imposed by the protein environment, the α carbon and two out of the three adjacent hydrogen atoms were frozen in all calculations, similarly to the procedures described by Roos and Siegbahn et al.[32,50] Four different models were explored: the active resting state (Fe_1−OH_2/$Y^\bullet$) and the predicted radical translocation product (Fe_1−OH/Y) of the cofactor, both with and without Y_{122} to account for the tyrosine's influence on the Mössbauer parameters. In addition, the met form (Fe_1−OH_2/Y) of the enzyme was modeled with Y_{122} and calculated for reference. Calculations were performed in the gas phase as well as in three distinct dielectric environments implemented via a conductor-like screening model (COSMO)[51] in the polarizable continuum model (PCM)[52] framework, termed as C-PCM, with ε = 4, 10, and 40. Optimizations were performed within the unrestricted DFT formalism with the three-parameter Becke−Lee−Yang−Parr (B3LYP) hybrid functional.[57,58] The antiferromagnetic coupling between the irons was achieved using broken-symmetry methods based on the ones developed by Noodleman.[48] Pople et al.'s 6-31g basis set[59] was used on all atoms except the irons, which were represented with the 6-311+g* basis set. Calculations of spectroscopic parameters were performed using the optimized geometries with the unrestricted DFT formalism using the ORCA[60] 2.9.1 package with the B3LYP functional and the 6-311g* basis set on all atoms. In the case of the iron atoms, a diffuse function was added to the basis set (6-311+g*). The broken symmetry state was realized via the "flipspin" feature implemented in ORCA. All ORCA calculations utilized the resolution of the identity Coulomb density fitting approximation[61] with the chain of spheres exchange (RIJCOSX).[62] The ^{57}Fe isomer shifts (δ) were calculated from the electron density at the iron nucleus ($\rho(0)$) using linear correlation response theory.[63,64] Calibration of $\rho(0)$ values was performed by correlating DFT calculated $\rho(0)$ values of iron complexes using the geometries presented by Römelt et al. with the experimental isomer shifts of these complexes.[65] The linear fit yielded the equation $\delta = 0.0963 - 0.3857\ (\rho(0) - 11616.5)$ with δ in mm/s and $\rho(0)$ in au^{-3}, and RMS = 0.9899 (Figure S5).

■ ASSOCIATED CONTENT

Supporting Information

Materials, protein production and purification, reconstitution of RNR-β with ^{57}Fe and/or ^{56}Fe, and activity assays. Alternative solution to fit the Mössbauer spectra of the N_3UDP-trapped radical translocation product (Figure S1). Mössbauer spectra of control samples lacking the stable radical translocation product (Figure S2). EPR spectra of site-selective labeled *E. coli* RNR before and after N_3UDP-induced trapping of the product of forward radical translocation (Figure S3). DFT optimized structures using COSMO with a dielectric constant of ε = 4 (Figure S4). Calibration of electron densities at the iron $\rho(0)$ (Figure S5). Parameters used to simulate the Mössbauer spectra (Table S1). Quantification of the different diiron and radical species in the samples (Table S2). DFT calculated quadrupole splittings (ΔE_Q), isomer shifts (δ), asymmetry parameters (η), and Fe_1−Fe_2 distances for the different diferric cofactor states (Table S3). Coordinates for optimized geometries of the investigated models calculated via COSMO with ε = 4. This material is available free of charge via the Internet at http://pubs.acs.org.

■ AUTHOR INFORMATION

Corresponding Author

ckrebs@psu.edu; jmb21@psu.edu; stubbe@mit.edu; alexey.silakov@gmail.com

Author Contributions

B.W., D.A.C., and K.Y. contributed equally.

Notes

The authors declare no competing financial interest.

■ ACKNOWLEDGMENTS

This work was supported by the National Institutes of Health (GM-55365 to J.M.B. and C.K.) and (GM-29595 to J.S.) and a postdoctoral fellowship of the Swiss National Science Foundation to B.W.

■ REFERENCES

(1) Stubbe, J.; van der Donk, W. A. *Chem. Rev.* **1998**, *98*, 705.
(2) Nordlund, P.; Reichard, P. *Annu. Rev. Biochem.* **2006**, *75*, 681.

(3) Stubbe, J.; Ackles, D. *J. Biol. Chem.* **1980**, *255*, 8027.
(4) Licht, S.; Gerfen, G. J.; Stubbe, J. *Science* **1996**, *271*, 477.
(5) Mao, S. S.; Yu, G. X.; Chalfoun, D.; Stubbe, J. *Biochemistry* **1992**, *31*, 9752.
(6) Stubbe, J.; Licht, S.; Gerfen, G.; Silva, D.; Booker, S. In *Vitamin B_{12} and B_{12}-proteins*; Kräutler, B., Arigoni, D., Golding, B. T., Eds.; Wiley-VCH: Weinheim, 1998; p 321.
(7) Uhlin, U.; Eklund, H. *Nature* **1994**, *370*, 533.
(8) Sintchak, M. D.; Arjara, G.; Kellogg, B. A.; Stubbe, J.; Drennan, C. L. *Nat. Struct. Biol.* **2002**, *9*, 293.
(9) Logan, D. T.; Andersson, J.; Sjöberg, B.-M.; Nordlund, P. *Science* **1999**, *283*, 1499.
(10) Ehrenberg, A.; Reichard, P. *J. Biol. Chem.* **1972**, *247*, 3485.
(11) Atkin, C. L.; Thelander, L.; Reichard, P.; Lang, G. *J. Biol. Chem.* **1973**, *248*, 7464.
(12) Sjöberg, B.-M.; Reichard, P.; Gräslund, A.; Ehrenberg, A. *J. Biol. Chem.* **1977**, *252*, 536.
(13) Sjöberg, B.-M.; Reichard, P.; Gräslund, A.; Ehrenberg, A. *J. Biol. Chem.* **1978**, *253*, 6863.
(14) Larsson, A.; Sjöberg, B.-M. *EMBO J.* **1986**, *5*, 2037.
(15) Stubbe, J.; Nocera, D. G.; Yee, C. S.; Chang, M. C. Y. *Chem. Rev.* **2003**, *103*, 2167.
(16) Ando, N.; Brignole, E. J.; Zimanyi, C. M.; Funk, M. A.; Yokoyama, K.; Asturias, F. J.; Stubbe, J.; Drennan, C. L. *Proc. Natl. Acad. Sci. U.S.A.* **2011**, *108*, 21046.
(17) Bennati, M.; Robblee, J. H.; Mugnaini, V.; Stubbe, J.; Freed, J. H.; Borbat, P. *J. Am. Chem. Soc.* **2005**, *127*, 15014.
(18) Bennati, M.; Weber, A.; Antonic, J.; Perlstein, L, D.; Robblee, J.; Stubbe, J. *J. Am. Chem. Soc.* **2003**, *125*, 14988.
(19) Seyedsayamdost, M. R.; Chan, C. T.; Mugnaini, V.; Stubbe, J.; Bennati, M. *J. Am. Chem. Soc.* **2007**, *129*, 15748.
(20) Ge, J.; Yu, G.; Ator, M. A.; Stubbe, J. *Biochemistry* **2003**, *42*, 10071.
(21) Seyedsayamdost, M. R.; Yee, C. S.; Reece, S. Y.; Nocera, D. G.; Stubbe, J. *J. Am. Chem. Soc.* **2006**, *128*, 1562.
(22) Seyedsayamdost, M. R.; Stubbe, J. *J. Am. Chem. Soc.* **2007**, *129*, 2226.
(23) Seyedsayamdost, M. R.; Xie, J.; Chan, C. T.; Schultz, P. G.; Stubbe, J. *J. Am. Chem. Soc.* **2007**, *129*, 15060.
(24) Seyedsayamdost, M. R.; Stubbe, J. *J. Am. Chem. Soc.* **2006**, *128*, 2522.
(25) Yokoyama, K.; Uhlin, U.; Stubbe, J. *J. Am. Chem. Soc.* **2010**, *132*, 15368.
(26) Yokoyama, K.; Smith, A. A.; Corzilius, B.; Griffin, R. G.; Stubbe, J. *J. Am. Chem. Soc.* **2011**, *133*, 18420.
(27) Climent, I.; Sjöberg, B.-M.; Huang, C. Y. *Biochemistry* **1992**, *31*, 4801.
(28) Ekberg, M.; Sahlin, M.; Eriksson, M.; Sjöberg, B.-M. *J. Biol. Chem.* **1996**, *271*, 20655.
(29) Reece, S. Y.; Hodgkiss, J. M.; Stubbe, J.; Nocera, D. G. *Philos. Trans. R. Soc., B* **2006**, *361*, 1351.
(30) Argirevic, T.; Riplinger, C.; Stubbe, J.; Neese, F.; Bennati, M. *J. Am. Chem. Soc.* **2012**, *134*, 17661.
(31) Ekberg, M.; Pötsch, S.; Sandin, E.; Thunnissen, M.; Nordlund, P.; Sahlin, M.; Sjöberg, B.-M. *J. Biol. Chem.* **1998**, *273*, 21003.
(32) Siegbahn, P. E. M.; Eriksson, L.; Himo, F.; Pavlov, M. *J. Phys. Chem. B* **1998**, *102*, 10622.
(33) Bollinger, J. M., Jr.; Edmondson, D. E.; Huynh, B. H.; Filley, J.; Norton, J. R.; Stubbe, J. *Science* **1991**, *253*, 292.
(34) Thelander, L.; Larsson, B.; Hobbs, J.; Eckstein, F. *J. Biol. Chem.* **1976**, *251*, 1398.
(35) Salowe, S. P.; Ator, M. A.; Stubbe, J. *Biochemistry* **1987**, *26*, 3408.
(36) Fritscher, J.; Artin, E.; Wnuk, S.; Bar, G.; Robblee, J. H.; Kacprzak, S.; Kaupp, M.; Griffin, R. G.; Bennati, M.; Stubbe, J. *J. Am. Chem. Soc.* **2005**, *127*, 7729.
(37) van der Donk, W. A.; Stubbe, J.; Gerfen, G. J.; Bellew, B. F.; Griffin, R. G. *J. Am. Chem. Soc.* **1995**, *117*, 8908.
(38) Preparations of *E. coli* β generally contain more $(Fe^{III})_2$ clusters than $Y_{122}^{\bullet}$. Metal analysis and $Y^{\bullet}$ quantification indicate that our preparation here contains 71% of active $(Fe^{III})_2/Y_{122}^{\bullet}$ β and 29% of the reduced, inactive $(Fe^{III})_2/Y_{122}$ (commonly referred to as "met") form, consistent with published results. Details of this quantification are provided in Table S2 of the Supporting Information. All % conversions determined by analysis of the Mössbauer spectra are reported here relative to the active $(Fe^{III})_2/Y_{122}^{\bullet}$ form rather than the total $(Fe^{III})_2$ cluster.
(39) Lynch, J. B.; Juarez-Garcia, C.; Münck, E.; Que, L., Jr. *J. Biol. Chem.* **1989**, *264*, 8091.
(40) Miller, M. A.; Gobena, F. T.; Kauffmann, K.; Münck, E.; Que, L., Jr.; Stankovich, M. T. *J. Am. Chem. Soc.* **1999**, *121*, 1096.
(41) Bollinger, J. M., Jr.; Chen, S.; Parkin, S. E.; Mangravite, L. M.; Ley, B. A.; Edmondson, D. E.; Huynh, B. H. *J. Am. Chem. Soc.* **1997**, *119*, 5976.
(42) Han, W. G.; Sandala, G. M.; Giammona, D. A.; Bashford, D.; Noodleman, L. *Dalton Trans.* **2011**, *40*, 11164.
(43) A second solution with $\delta_1 = 0.47$ mm/s, $\Delta E_{Q1} = 1.97$ mm/s and $\delta_2 = 0.53$ mm/s, $\Delta E_{Q2} = 1.68$ mm/s) fits the data equally well. Experiments with preparations of β in which the Mössbauer-active ^{57}Fe was enriched in Fe_1 or Fe_2 showed that the parameters quoted in the main manuscript fit the data slightly better. However, we cannot determine with certainty which solution is the correct one (Figure S1).
(44) Münck, E. In *Physical Methods in Bioinorganic Chemistry*; Que, L., Jr., Ed.; University Science Books: Sausalito, CA, 2000; p 287.
(45) Kurtz, D. M. *Chem. Rev.* **1990**, *90*, 585.
(46) Karlsson, M.; Sahlin, M.; Sjöberg, B.-M. *J. Biol. Chem.* **1992**, *267*, 12622.
(47) DeFelippis, M. R.; Murthy, C. P.; Broitman, F.; Weinraub, D.; Faraggi, M.; Klapper, M. H. *J. Phys. Chem.* **1991**, *95*, 3416.
(48) Noodleman, L. *J. Chem. Phys.* **1981**, *74*, 5737.
(49) Högbom, M.; Galander, M.; Andersson, M.; Kolberg, M.; Hofbauer, W.; Lassmann, G.; Nordlund, P.; Lendzian, F. *Proc. Natl. Acad. Sci. U.S.A.* **2003**, *100*, 3209.
(50) Roos, K.; Siegbahn, P. E. M. *J. Biol. Inorg. Chem.* **2011**, *16*, 553.
(51) Klamt, A.; Schüürmann, G. *J. Chem. Soc., Perkin Trans.* **1993**, *2*, 799.
(52) Cossi, M.; Rega, N.; Scalmani, G.; Barone, V. *J. Comput. Chem.* **2003**, *24*, 669.
(53) Salowe, S.; Bollinger, J. M., Jr.; Ator, M.; Stubbe, J.; McCracken, J.; Peisach, J.; Samano, M. C.; Robins, M. J. *Biochemistry* **1993**, *32*, 12749.
(54) Malmström, B. G.; Reinhammar, B.; Vänngård, T. *Biochim. Biophys. Acta* **1970**, *205*, 48.
(55) Aasa, R.; Vänngård, T. *J. Magn. Reson.* **1975**, *19*, 308.
(56) Frisch, M. J.; Trucks, G. W.; Schlegel, H. B.; Scuseria, G. E.; Robb, M. A.; Cheeseman, J. R.; Scalmani, G.; Barone, V.; Mennucci, B.; Petersson, G. A.; Nakatsuji, H.; Caricato, M.; Li, X.; Hratchian, H. P.; Izmaylov, A. F.; Bloino, J.; Zheng, G.; Sonnenberg, J. L.; Hada, M.; Ehara, M.; Toyota, K.; Fukuda, R.; Hasegawa, J.; Ishida, M.; Nakajima, T.; Honda, Y.; Kitao, O.; Nakai, H.; Vreven, T.; Montgomery, J. A., Jr.; Peralta, J. E.; Ogliaro, F.; Bearpark, M.; Heyd, J. J.; Brothers, E.; Kudin, K. N.; Staroverov, V. N.; Kobayashi, R.; Normand, J.; Raghavachari, K.; Rendell, A.; Burant, J. C.; Iyengar, S. S.; Tomasi, J.; Cossi, M.; Rega, N.; Millam, J. M.; Klene, M.; Knox, J. E.; Cross, J. B.; Bakken, V.; Adamo, C.; Jaramillo, J.; Gomperts, R.; Stratmann, R. E.; Yazyev, O.; Austin, A. J.; Cammi, R.; Pomelli, C.; Ochterski, J. W.; Martin, R. L.; Morokuma, K.; Zakrzewski, V. G.; Voth, G. A.; Salvador, P.; Dannenberg, J. J.; Dapprich, S.; Daniels, A. D.; Farkas, Ö.; Foresman, J. B.; Ortiz, J. V.; Cioslowski, J.; Fox, D. J. *Gaussian 09*, Revision C.01, Gaussian, Inc.: Wallingford, CT, 2009.
(57) Becke, A. D. *J. Chem. Phys.* **1993**, *98*, 5648.
(58) Lee, C.; Yang, W.; Parr, R. G. *Phys. Rev. B: Condens. Matter* **1988**, *37*, 785.
(59) Krishnan, R.; Binkley, J. S.; Seeger, R.; Pople, J. A. *J. Chem. Phys.* **1980**, *72*, 650.
(60) Neese, F. *WIREs Comput. Mol. Sci.* **2012**, *2*, 73.
(61) Neese, F. *J. Comput. Chem.* **2003**, *24*, 1740.

(62) Neese, F.; Wennmohs, F.; Hansen, A.; Becker, U. *Chem. Phys.* **2009**, *356*, 98.
(63) Filatov, M. *J. Chem. Phys.* **2007**, *127*, 084101.
(64) Sinnecker, S.; Slep, L. D.; Bill, E.; Neese, F. *Inorg. Chem.* **2005**, *44*, 2245.
(65) Römelt, M.; Ye, S.; Neese, F. *Inorg. Chem.* **2009**, *48*, 784.